ARMY RESEARCH LABORATORY

Direct Fuel Injector Power Drive System Optimization

by Xiaohua Zhang, Alan Palazzolo, Chol-Bum Kweon, Erwin Thomas, Randall Tucker, and Albert Kascak

ARL-RP-484 **June 2014**

A reprint from *SAE Int. J. Engines*, Vol. 7, no. 3, August 2014.

NOTICES

Disclaimers

The findings in this report are not to be construed as an official Department of the Army position unless so designated by other authorized documents.

Citation of manufacturer's or trade names does not constitute an official endorsement or approval of the use thereof.

Destroy this report when it is no longer needed. Do not return it to the originator.

Army Research Laboratory
Aberdeen Proving Ground, MD 21005-5066

ARL-RP-484 **June 2014**

Direct Fuel Injector Power Drive System Optimization

Xiaohua Zhang, Alan Palazzolo, Erwin Thomas, and Randall Tucker
Texas A&M University

Chol-Bum Kweon
Vehicle Technology Directorate, ARL

Albert Kascak
Vehicle Technology Directorate, ARL (retired)

A reprint from *SAE Int. J. Engines*, Vol. 7, no. 3, August 2014.

REPORT DOCUMENTATION PAGE	Form Approved OMB No. 0704-0188

1. REPORT DATE *(DD-MM-YYYY)*	2. REPORT TYPE	3. DATES COVERED (From - To)
June 2014	Reprint	1 January 2013–31 August 2013

4. TITLE AND SUBTITLE
Direct Fuel Injector Power Drive System Optimization

5a. CONTRACT NUMBER
W911NF-10-2-0036

5b. GRANT NUMBER

5c. PROGRAM ELEMENT NUMBER

6. AUTHOR(S)
Xiaohua Zhang, Alan Palazzolo, Erwin Thomas, Randall Tucker, Chol-Bum Kweon, and Albert Kascak

5d. PROJECT NUMBER

5e. TASK NUMBER

5f. WORK UNIT NUMBER

7. PERFORMING ORGANIZATION NAME(S) AND ADDRESS(ES)
U.S. Army Research Laboratory
ATTN: RDRL-VTP
Aberdeen Proving Ground, MD 21005-5066

8. PERFORMING ORGANIZATION REPORT NUMBER
ARL-RP-484

9. SPONSORING/MONITORING AGENCY NAME(S) AND ADDRESS(ES)

10. SPONSOR/MONITOR'S ACRONYM(S)

11. SPONSOR/MONITOR'S REPORT NUMBER(S)

12. DISTRIBUTION/AVAILABILITY STATEMENT
Approved for public release; distribution is unlimited.

13. SUPPLEMENTARY NOTES
A reprint from *SAE Int. J. Engines*, Vol. 7, no. 3, August 2014.

14. ABSTRACT
The objective of this study is to optimize the injector power drive system for improved fuel injection quantity and timing control. The power drive system was optimized for improved injection repeatability under different operating conditions such as fuel supply pressures. A coupled simulation of injector electromagnetic, pintle (needle) rigid body motion and computational fluid dynamics (CFD) model was employed to generate the optimal values of the 1st stage current, the 1st stage on-time and the 2nd stage current. The simulation results were validated against the experimental data measured with a photo detector measurement system.

15. SUBJECT TERMS
fuel injector, JP-8, injector drive, optimization, spray

16. SECURITY CLASSIFICATION OF:			17. LIMITATION OF ABSTRACT	18. NUMBER OF PAGES	19a. NAME OF RESPONSIBLE PERSON
a. REPORT	b. ABSTRACT	c. THIS PAGE			Xiaohua Zhang
Unclassified	Unclassified	Unclassified	UU	24	19b. TELEPHONE NUMBER (*Include area code*) 410-278-9319

Standard Form 298 (Rev. 8/98)
Prescribed by ANSI Std. Z39.18

2014-01-1442
Published 04/01/2014

doi:10.4271/2014-01-1442
saeeng.saejournals.org

Direct Fuel Injector Power Drive System Optimization

Xiaohua Zhang and Alan Palazzolo
Texas A&M University

Chol-Bum Kweon
U.S. Army Research Laboratory

Erwin Thomas and Randall Tucker
Texas A&M University

Albert Kascak
U.S. Army Research Laboratory (retired)

ABSTRACT

The objective of this study is to optimize the injector power drive system for improved fuel injection quantity and timing control. The power drive system was optimized for improved injection repeatability under different operating conditions such as fuel supply pressures. A coupled simulation of injector electromagnetic, pintle (needle) rigid body motion and computational fluid dynamics (CFD) model was employed to generate the optimal values of the 1st stage current, the 1st stage on-time and the 2nd stage current. The simulation results were validated against the experimental data measured with a photo detector measurement system.

CITATION: Zhang, X., Palazzolo, A., Kweon, C., Thomas, E. et al., "Direct Fuel Injector Power Drive System Optimization," *SAE Int. J. Engines* 7(3):2014, doi:10.4271/2014-01-1442.

INTRODUCTION

Direct fuel injectors have rapidly replaced carburetors and manifold fuel injectors in modern internal combustion (IC) engines. With a direct fuel injection system, high-pressure fuel is directly sprayed into a combustion chamber. The most common fuel injector actuator is a solenoid type, which converts electrical energy into mechanical motion through electromagnetics. A pintle valve inside the injector is used to electronically control the opening and closing of the nozzle. The motion of the pintle (needle), which acts as a plunger in the solenoid, defines the temporal characteristics of a spray, i.e. opening delay time, closing delay time, spray duration and its rate shape. These temporal spray characteristics are important parameters in an Engine Control Unit (ECU), which contains tables with injection timing and duration for optimal combustion and emission control under different engine operating conditions. The ECU determines required injection duration per requested fuel injection quantity from the injection duration table. Then, the ECU sends a control signal to the fuel injection power module, which sends a current signal to the injector solenoid coil to create magnetic field in the stator. Then, the stator pulls the pintle to open the injector nozzle. This pintle movement occurs when the magnetic force overcomes the opposing forces, i.e. pressure, spring compression and pintle valve contact friction forces.

The physics involved in the fuel injector pintle movement is a complex combination of electromagnetic, fluid dynamics and coupled motion with pintle and valve structures where the injector power drive system plays a key role in the dynamics of the pintle. Desired pintle dynamics should have the following characteristics: (1) fast response, (2) repeatability, and (3) least power consumption.

Fast response implies short opening and closing delay times which are critical in modern IC engines because fuel injection should be made at optimal timing in narrow window. Combustion is optimized when fuel is injected at optimal timing at each operating condition. Optimal injection timing is determined for best combinations of engine performance, efficiency and emissions, considering fuel-air mixing time, ignition delay time and dwell time. Dwell time is defined as the time between the end of injection and the start of combustion. In modern compression-ignition direct injection (CIDI) engines, injection timing ranges from several degrees before to near top dead center (TDC) depending on the engine operating

conditions. Injection timing is typically retarded as engine load is increased. Pilot injection strategies have been widely used to reduce combustion noise and improve engine idling. Typical pilot injection quantities range from about 1 to 5 mg for advanced diesel engines. Fast pintle movement is critical in multiple injections because multiple injections should be made in each cycle, while the first injection minimally influencing the following injection. Increasing the current ramp rate of the solenoid coil would increase the pulling motion of the pintle, given that in theory the magnetic force is proportional to the square of supply current to the injector. In reality, however, it will reach a point where increasing the magnetic force rate is impeded by the limited current increasing rate, which is determined by inductance. Other factors such as hydraulic hysteresis, magnetization hysteresis and saturation of the magnetic material also impose limitations on pintle response time.

Repeatable fuel injection leads to less shot-to-shot variations of fuel injection quantity and injection rate. Repeatable fuel injection can be achieved when the pintle moves rapidly to a desired position (typically fully open position) to avoid random fuel injection quantity and rate. Higher current may ensure the repeatability of the injection by creating more than enough magnetic force to hold the pintle at its desired position.

However, higher current would create more heat in the solenoid coil, which increases the temperature of the surrounding magnetic material, thus degrading the magnetic material property, i.e. lowered saturation limit and more hysteresis. Injector performance is highly dependent on temperature in the solenoid which was observed during our injector dry test in which the threshold current increased significantly as the injector body temperature was increased. Ideally, an injector power drive system should use the least amount of current, while achieving fast response and repeatable pintle movement.

In the past, research has been performed mostly in two different areas: (1) numerical modeling of fuel injector dynamics and (2) power drive design for direct fuel injectors that typically deal with power strategies to the injector solenoid coil. Numerical simulation codes for diesel injection systems were developed by various authors [1, 3, 4]. All these codes include or partially include coupled multi-physics model of hydraulics, fluid, mechanical and electromagnetic. Digesu's model coupled one-dimensional hydraulics with a two-dimensional (2D) axisymmetric electromagnetic finite element code to provide magnetic force in terms of exciting current and working gap [1]. In his study, needle lift, pressures (pipes, control volume, rail and accumulative volume) and flow rate were matched with experimental data. The authors investigated how pipe design affects the needle lift profile due to the hydraulic wave, and showed a moderate dependence on pipe parameters. Ficarella developed a code to evaluate the instability phenomena in a common rail injection system to predict injection characteristics [2]. It was found that the most challenging part of the modeling lies in the control valve whose residual motion causes re-opening of the valve after a pilot injection. Coppo's code was also based on a common-rail injector with a combined pipe, fluid, mechanical and electromagnetic model [3, 4]. Experimentally measured exciting current signals were input into the model, which included magnetic saturation effects. Good agreement was observed between calculated and experimental profiles of rail pressure, needle lift, and injection quantity. Hu developed a one-dimensional (1D) model to correlate the pressure profile with the measured one in which no electromagnetic model was used and a measured magnetic force profile was employed in the 1D model [5]. Ando developed a 1D electromagnetic model coupled with simplified rigid body and fluid models [6]. The main emphasis of this model was on the electromagnetic effects including magnetization time lag.

For power drive optimization, Tsai designed a three-stage electrical drive for high-pressure gasoline direct injection (GDI) injectors. In the design, the first two stages used a power Metal-Oxide-Semiconductor Field-Effect Transistor (MOSFET) to switch between power supplies, while the 3rd stage used pulse-width-modulation (PWM) control. The author provided the current amperages for each stage (12/5/3A) but did not fully explain why those values were chosen. The author observed that the pintle closed faster with the 3rd stage PWM control than with a direct voltage control method [7]. Tsai, in another paper, performed a parametric study to investigate the effect of voltage, current, frequency and fuel pressure on injection quantity [8].

From the literature review, it was found that there is a lack of integral method to model from injector power source to pintle dynamics, as well as driver design details for controlling fuel injectors. The goal of this paper is to find the optimal power strategy to drive fuel injectors, specifically in our case, it is a gasoline direct fuel injector (GDFI). The methodology of fulfilling this goal is as follows: using electromagnetic-mechanical-fluid coupled simulation to reveal the impact of injector current shapes on injection dynamics, as well as to achieve fast response and repeatability of pintle movement with the least power consumption or the minimal driving current. Through fluid and mechanical model, the electromagnetic force requirement is formed; and through electromagnetic circuit analysis, the corresponding current requirement, which contains optimal parameters for multi-stage current shape, is established under different supply pressures. Finally, the simulation results are validated using a photo detector system.

The paper is organized as follows: Firstly, injector power drive system basics, electromagnetic system, mechanical system and fluid system are introduced separately in four different sections. These four sections are the building blocks for the entire system. Secondly, a coupled simulation is run using one of the power strategies (current shapes) to reveal the detailed dynamics of pintle movement, flow rate and pressure forces on the pintle under different supply pressures. The insight of current requirement is gained after this run of simulation.

Thirdly, two more power strategies (current shapes) are applied to illustrate the failure of maintaining the injection repeatability if the current requirement is violated. Fourthly, the optimal power strategy is discussed in detail, which includes the reason of using the multi-stage current shape and its optimal parameter settings. Lastly, the simulation results are validated using a photo detector system.

Injector Power Drive System Basics

Direct fuel injectors are designed for fast response under high pressures, which requires careful selection of their power drives. The power input to the injector coil creates a magnetic force to open the pintle valve. Since magnetic force is proportional to the square of supply current, the pintle will only move when supply current reaches certain levels where magnetic force overcomes opposing forces (including pressure, spring and friction forces). The threshold of the pintle movement depends on the threshold level of the excitation current in the solenoid coil. Therefore, how fast the pintle opens depends on how fast the current level can reach the required current threshold. However, there is always a time constant for current rise due to the inductance in the solenoid coil. The current rising rate needs to be fast to achieve fast opening of the pintle.

The governing equation for a simple resistor-inductor circuit (RL circuit) is

$$V = i \cdot R + L \cdot \frac{di}{dt} \tag{1}$$

where V is the voltage across the coil; R is the resistance; and L is the inductance. The step voltage input response of the current is obtained by solving (1) to obtain:

$$i(t) = \frac{V}{R} \cdot (1 - e^{-\frac{R}{L} \cdot t}) = \frac{V}{R} \cdot (1 - e^{-\frac{1}{\tau} \cdot t}) \tag{2}$$

where $\frac{L}{R}$ is the electrical subsystem time constant τ. The inductance was measured to be 1.9 millihenry (mH) at 1 kHz and 3.9 mH at 0.12 kHz at the maximum air gap. In our case,

$$\tau = \frac{L}{R} = \frac{(1.9 \sim 3.9)mH}{1.5\Omega} = 1.26 \sim 2.6ms \tag{3}$$

This means that it takes 1.26~2.6 ms to reach 63.2% of the steady-state current $\frac{V}{R}$; where R, L are measured values.

Figure 1 illustrates the times to reach 8.5 A for different voltage inputs. The reason for 8.5 A in the analysis will be discussed in the later section where the magnetic force requirement is specified.

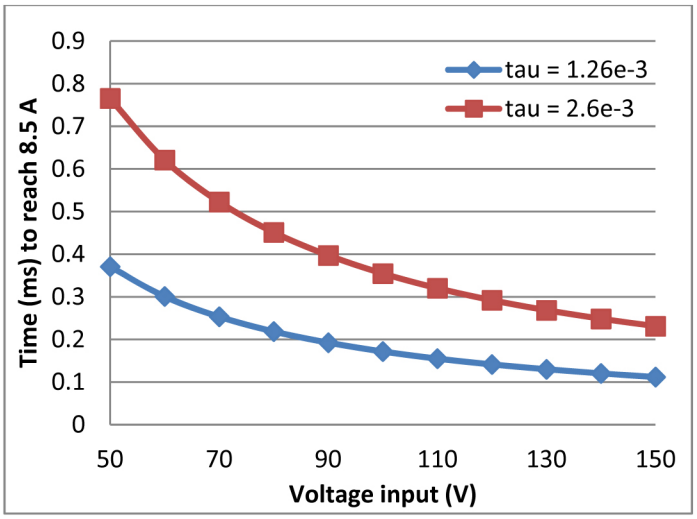

Figure 1. Time to reach 8.5 A with different time constants

A PWM servo-power amplifier was used to provide current to the fuel injectors. Nowadays, PWM amplifiers become the preferred way of driving fuel injectors. Compared with power MOSFETs, PWM power amplifiers are more power efficient and easier to use.

A PWM power amplifier consists of a DC power supply, capacitor (for short pulsation application), and control signal. The DC power supply delivers power to the PWM via the capacitor. Through the PWM frequency and duty cycle, the output current (or voltage) is modulated to match the input control signal shape at higher power level. For instance, in our system, 0~10 volts control signal was fed into PWM and the output from the PWM was 0~15 A current shape that closely followed the input control signal. This approach is extremely helpful because real applications utilize complex control strategies of the fuel injectors. One of the main benefits of a PWM amplifier is that one can easily adjust the control signal amplitude and time duration with multiple stages to regulate the multiple stage current output to the fuel injector. Another benefit of the PWM control was discussed in Tsai's paper [7] which showed that the last stage PWM control could shorten the closing delay time of the fuel injector pintle. Figure 2 illustrates the injector power and control system utilized in the present paper.

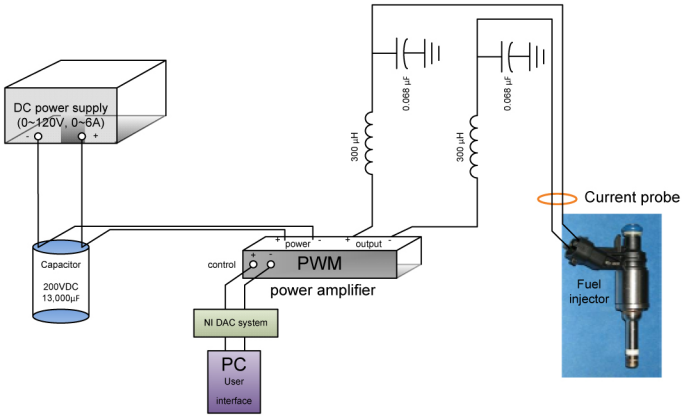

Figure 2. Injector power and control system

Electromagnetic System

Electromagnetic analysis is an essential part of the multi-physics model. The fuel injector used in this study is a BOSCH GDI injector (HDEV 5.2), which is a plunger type solenoid electromagnetic device. A coil is imbedded inside the injector body, with a magnetic conducting material forming a closed magnetic path when the coil is energized. The motion of the pintle is caused by the magnetic field created by the current flowing in the coil.

The electromagnetic model includes an electrical circuit model for the injector coil and a magnetic model for magnetic flux and force calculation.

The electrical circuit for the injector coil is basically a RL circuit. The PWM power amplifier was not modeled in this study due to the circuit's low frequency nature compared to the switching frequency of PWM, which is 22 kHz in our case. For direct comparison, the time constant of the injector RL circuit is about 2 ms, while the switching time is only 0.02 ms. Thus, the model was simplified to use three power sources: one voltage source with a time-controlled switch, together with two pulse current sources, to obtain a two-stage current shape. In the actual system, a two-stage control voltage signal is fed into the PWM power amplifier and then the output is a two-stage current shape. The electrical properties of the fuel injector coil and PWM power amplifier are listed in Table 1.

The electrical circuit was modeled in Maxwell circuit editor, as shown in Figure 3. It included a voltage source with a switch controlling on and off time, a pulse current source for the peak current, and another pulse current source for the holding current. This circuit model was imported into a 2D axisymmetric finite element code Maxwell as external excitation source for the coil. The time constant τ in the RL circuit (see equation 3) determines the maximum current increasing rate. The inductance, which is represented as winding1 in the circuit, changes as the geometry changes, which takes into account of the pintle motion in the magnetic circuit. Figure 4 shows the inductance profile with respect to the change of air gap. The inductance from Maxwell was calculated through the relationship $L = \frac{d\lambda}{di}$ at each time step in the transient analysis. It is shown that the change of the inductance due to pintle motion counts for about 10% of coil's total inductance.

Table 1. Electrical properties of the fuel injector coil and PWM power amplifier used in this study

Resistance		1.5 Ω
Inductance		1.9 mH at 1 kHz; 3.9 mH at 0.12 kHz
Number of turns		160
PWM switching frequency		22 kHz
PWM power range	Peak current	50 A
	Continuous current	25 A
	Supply voltage	40-190 VDC

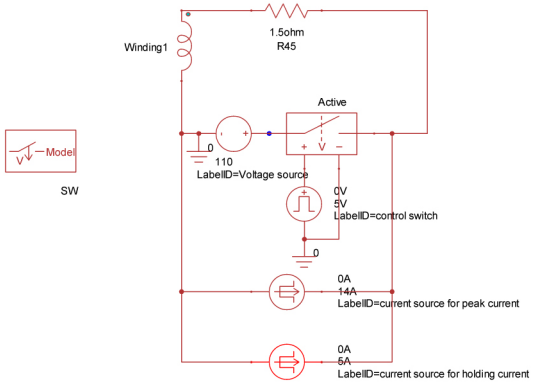

Figure 3. Electrical circuit in Maxwell circuit editor.

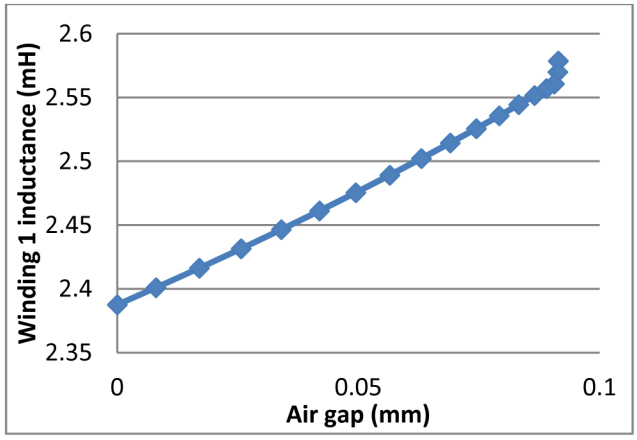

Figure 4. Inductance at different air gaps from Maxwell.

This inductance plays an important role in determining the current rise time. A 1D magnetic analysis is provided below to compare with the inductance calculation from Maxwell.

From Ampere's law $\oint_c \vec{H} \times d\vec{l} = I_{net}$

$$H_1 \cdot \Delta x + H_2 \cdot w + H_3 \cdot w = N \cdot I \quad (4)$$

where, the parameters in Equation (4) are illustrated in Figure 5.

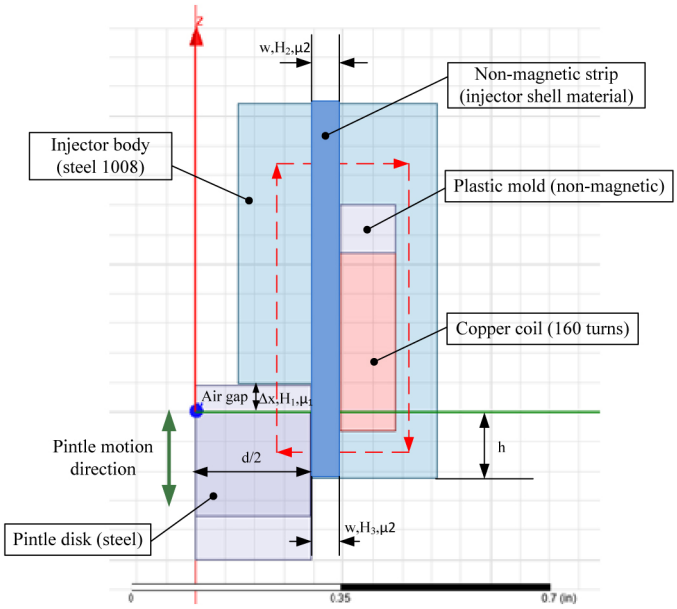

Figure 5. Flux path in the magnetic circuit analysis

Apply Gauss M around pintle disk, $\iint_s \vec{B} \times d\vec{a} = 0$

which yields

$$\mu_1 \cdot H_1 \cdot \frac{\pi}{4} d^2 - \mu_2 \cdot H_3 \cdot \pi d \cdot h = 0 \tag{5}$$

Assume no fringing and leakage,

$$H_2 \cong H_3 \tag{6}$$

Also, the permeability in the air μ_1 and the one in the non-magnetic strip μ_2 are similar: $\mu_1 \approx \mu_2$;

Apply flux linkage $\lambda = N \cdot \int_s \vec{B} \times d\vec{a}$ on the top plane of the pintle disk,

$$\lambda = \left[\frac{N^2 \cdot \mu_1 \cdot \frac{\pi}{4} \cdot d^2 \cdot h}{\frac{d \cdot w}{2} + \Delta x \cdot h} \right] \cdot i \tag{7}$$

$$L = \frac{N^2 \cdot \mu_1 \cdot \frac{\pi}{4} \cdot d^2 \cdot h}{\frac{d \cdot w}{2} + \Delta x \cdot h}$$

where, inductance .

The geometric parameters were obtained by measuring the dimensions with a cut-open injector. Table 2 lists the parameters used in the calculation. The calculated inductance (2.4 ~ 2.6 mH) correlates well with the measured inductance, which ranged from 1.9 mH at 1 kHz to 3.9 mH at 0.12 kHz.

Table 2. Parameters for inductance calculation

Non-magnetic strip width w [mm]	0.8
Pintle disk diameter d [mm]	10
Pintle height h [mm]	4
Air gap Δx [mm]	0 ~ 0.1
Permeability μ_1 [H/m]	1.256e-6
Number of coil turns	160
Calculated inductance using eqn (7) [mH]	2.4 ~ 2.6

Figure 6 shows elapsed times for different current targets at the calculated inductances with the same 110 V voltage source using Equation (2).

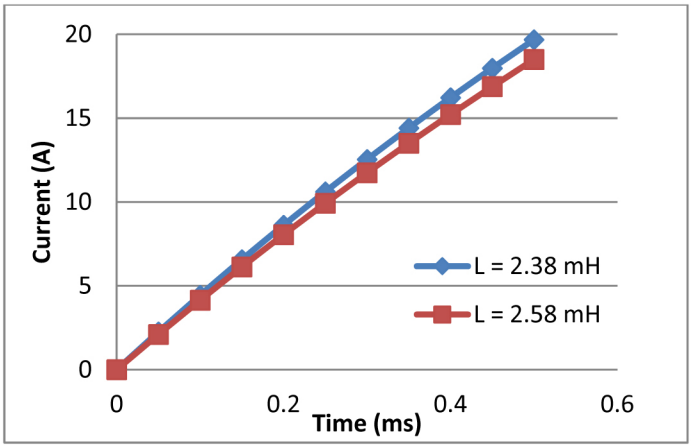

Figure 6. Current level vs. elapsed times at the calculated inductances

Figure 7 compares the calculated current shape from Maxwell and the measured one with the 1st stage on-time of 400 μs and 2nd stage on-time of 600 μs. The calculated current profile, especially the rise time (which is the key to the opening delay time), fits well with the measured current.

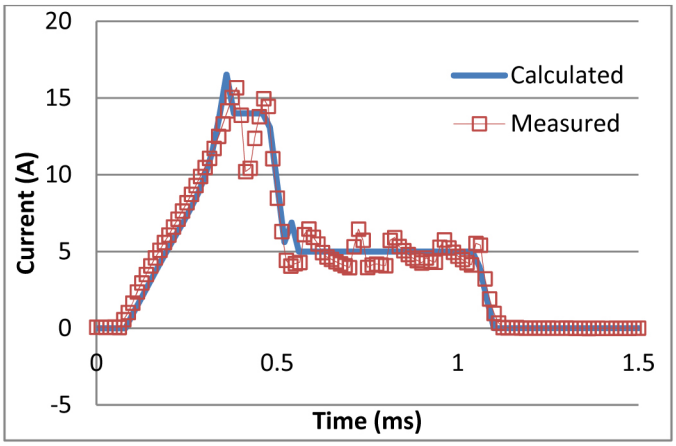

Figure 7. Maxwell calculated and measured current shapes

In the electrical circuit simulation, the current limit was set by the PWM power amplifier and the voltage source was turned off when the current reached the current limit. This was done to capture the characteristics of the rising curve and the current limit. Another pulse current source was used to provide the 2nd stage current. In practice, once a desired current shape is determined, it is relatively easy to adjust the current magnitude and duration by changing the DC power supply voltage, control signal amplitude, current limit and command signal's time durations.

In Figure 8, the 2D axisymmetric model in Maxwell shown in Figure 5 was simulated in transient. Magnetic density B vector plot was shown at time t = 0.4 ms at which the 1st stage current reached its steady-state.

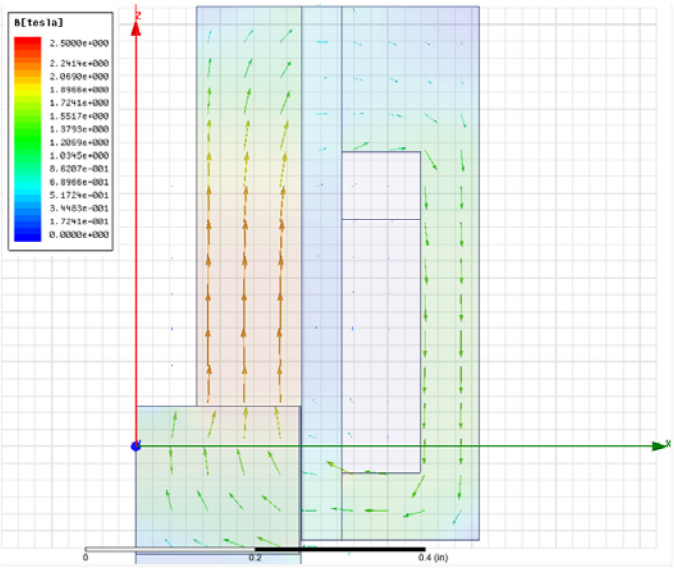

Figure 8. Magnetic flux density vector plot at t = 0.4 ms from 2D Maxwell transient with the two-stage current shown in Figure 7

The magnetic field density was calculated using the ampere's law and the constitutive relationship between flux density B and magnetic field strength H: $B = \mu \cdot H$. Then, Maxwell force law was used to calculate the magnetic force, given the magnetic flux density, permeability and area.

$$F_{mag} = \frac{B^2 A}{2\mu} = \frac{(\mu \cdot H_1)^2 A}{2\mu} \tag{8}$$

where, B is the flux density at H_1; A is the area on the upper surface of pintle disk; μ is the permeability of air.

Solving Equations (4, 5, 6) for H_1, then substituting H_1 into Equation (8), the magnetic force becomes

$$F_{mag} = \frac{\mu \cdot N^2 \cdot h^2 \cdot A}{2\left(\frac{d \cdot w}{2} + \Delta x \cdot h\right)^2} \cdot i^2 \tag{9}$$

The magnetic force was also calculated using the finite element code Maxwell. Figure 9 compares the magnetic forces calculated with Equation (9) and Maxwell at different air gaps and current levels.

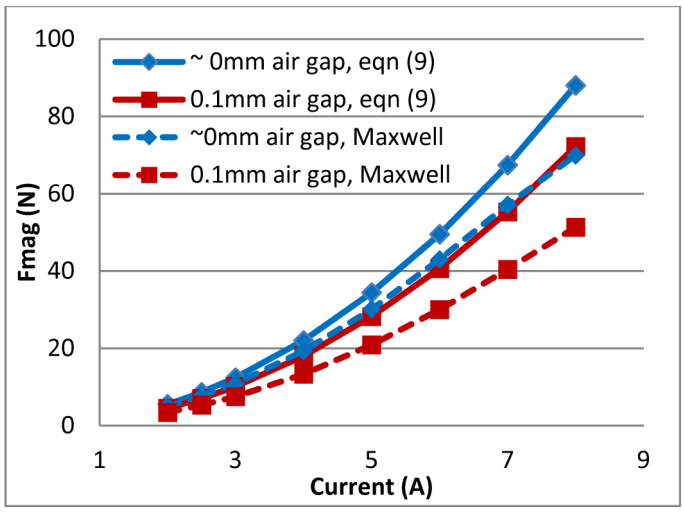

Figure 9. Calculated magnetic forces at different air gaps and current levels with Equation (9) and Maxwell

The 2D axisymmetric finite element code Maxwell considered the non-linearity of the B-H curve of the magnetic material and the fringing loss. Therefore, the magnetic force calculated using Maxwell was less than the theoretical force calculated from Equation (9) as excitation current increased. However, the two force curves are close enough to justify the results from Maxwell.

Figure 9 shows the magnetic forces calculated using finite element code Maxwell with the current shape shown in Figure 7 under three different conditions: with pintle motion and without pintle motion at extreme pintle positions.

Figure 10 shows that the magnetic force with moving pintle (solid) falls in-between the magnetic forces at extreme pintle positions without pintle motion (dotted and dashed). For simplicity, the magnetic force with non-moving pintle at its minimum air gap (~0mm) was used in the following coupled analysis assuming that the magnetic force is only a function of time given a certain current shape.

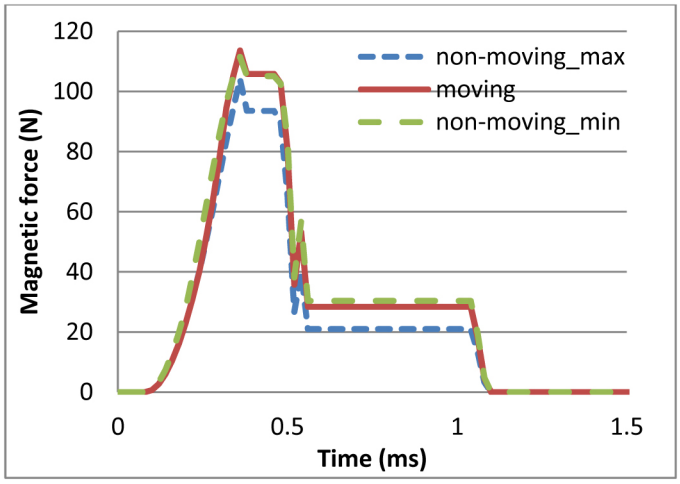

Figure 10. Magnetic force profile with and without pintle movement using Maxwell

Besides current and air gap, another important factor that affects the magnetic force is the magnetic saturation. The magnetic saturation imposes the maximum resultant magnetic force due to the flux saturation in the magnetic circuit. Therefore, the magnetic force cannot increase infinitely with the increasing current. Figure 11 shows the magnetic forces at different currents, pintle positions, and saturation levels. Amp*turns is the multiplication of current (amp) and coil's number of turns. In our case, the total number of turns was 160.

The resultant magnetic forces of less than 1000 amp-turns were similar for different saturation materials. However, the difference of the resultant magnetic forces could be as much as 15 N at the same current (1500 amp*turns) and air gap (0.1mm), only with the change of magnetic material from 1.5 Tesla (T) saturation to 2 T saturation. Therefore, in order to obtain the largest possible magnetic force, it is preferred to use high saturation material in the magnetic path.

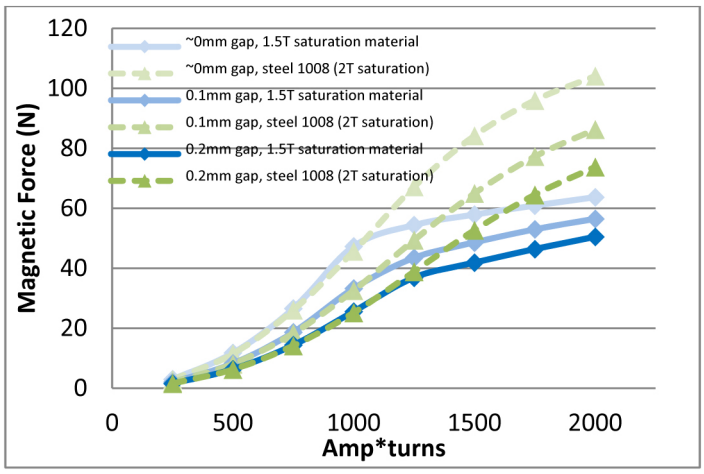

Figure 11. Saturation study for different materials and air gaps

Figure 12 shows the magnetic force versus the current (Amp*turns) using steel 1008 with 0.1 mm air gap. 1250 amp*turns (7.8 A at 160 turns) created about 50 N magnetic force.

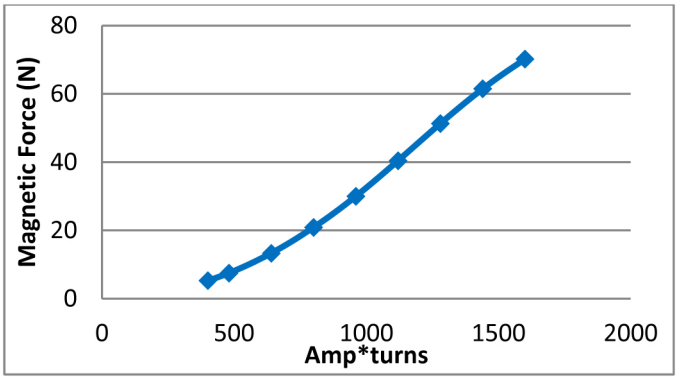

Figure 12. Magnetic force vs. current at 0.1 mm air gap with steel 1008 (2T saturation)

Mechanical System

The mechanical system model predicts the rigid body motion of the pintle. The force illustration is shown in Figure 13. At the beginning, the pintle sits on the valve seat where there are five forces acting on it: pressure, gravity, spring, contact friction and supporting forces. The pressure force is due to the pressure on the pintle. Spring force is due to the return spring's compression. Contact friction force takes into account of the initial friction due to its contact with the valve seat. And the support force from valve seat, represented as spring and damper, is the equal and opposite force of all other forces when pintle rests on the pintle valve. The magnetic force increases as the current in the coil increases. In the event of pintle movement, magnetic force overcomes pressure, gravity, spring and contact friction forces. The pintle motion is limited by the stator, which is represented as another set of spring and damper at the distance of 0.09mm. This distance was measured with a miniature dial indicator in the event of pintle motion under the condition where there was no fluid inside the fuel injector.

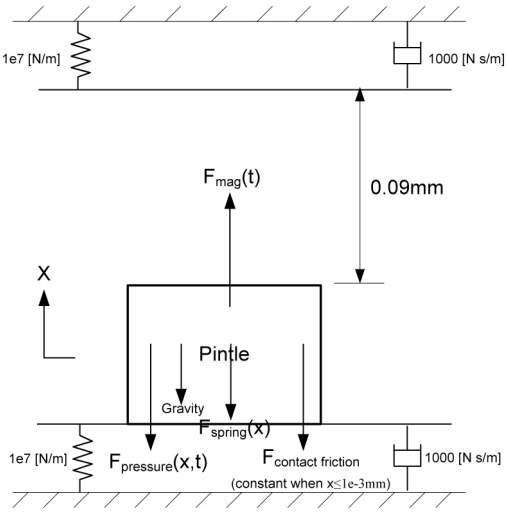

Figure 13. Mechanical system of the pintle with force illustration

The non-moving pintle at ~0mm air gap with steel 1008 and power strategy shown in Figure 7 was used to create the magnetic force profile shown in Figure 14. The magnetic force $F_{mag}(t)$ can be expressed by segmenting the force profile and curve-fitting at different segments:

$$F_{mag}(t)=\begin{cases}0, & 0ms<t<0.08ms\\ 110.6\cdot e^{-\left(\frac{t-0.3823}{0.1241}\right)^2}+20.68\cdot e^{-\left(\frac{t-0.2471}{0.08861}\right)^2}, & 0.08ms<t<0.37ms\\ 105, & 0.37ms<t<0.47ms\\ -914.9\cdot t+536.9, & 0.47ms<t<0.55ms\\ 30.35, & 0.55ms<t<1.05ms\\ -528.5\cdot t+579.1, & 1.05ms<t<1.09ms\\ 0, & t>1.09ms\end{cases} \quad (10)$$

where t in the expression is in [ms].

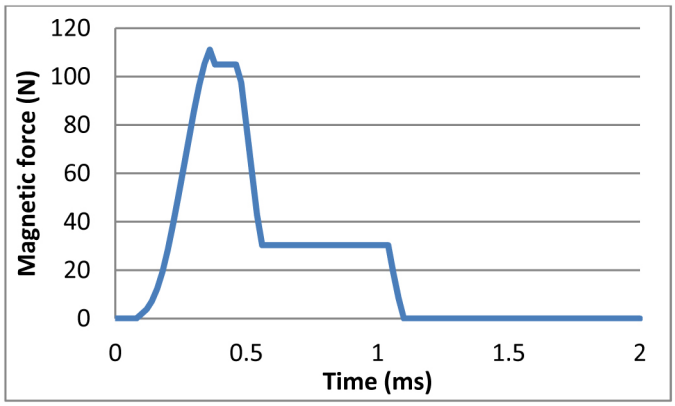

Figure 14. Magnetic force profile

The spring force F_{spring} can be expressed as,

$$F_{spring}(x)=F_0+K_{spring}\cdot x \quad (11)$$

where, F_0 = −6.5 *N* is the initial compression force; K_{spring} = −12140 [*N* / *m*] is the spring constant, which is obtained by performing the return spring test.

The initial contact friction force is,

$$F_{initial\ contact\ friction}(x)=\begin{cases}-13.8\ N, & x\le 1e-3mm\\ 0, & x>1e-3mm\end{cases} \quad (12)$$

The initial spring compression and initial contact friction forces were determined by performing the threshold current test which was conducted to investigate the minimum current to open the pintle valve under non-fluid condition. This single valued friction force may change as the fluid pressure applies. Future high fidelity model should investigate further on this force.

When the pintle moves 0.09 mm distance upwardly, a barrier is enforced by applying a stiff spring and damper to simulate that the pintle hits the stator. The force acting on pintle from the upper wall can be expressed mathematically as follows,

$$F_{upper\ wall}(x)=\begin{cases}-K*(x-0.09mm)-c*\dot{x}, & x>0.09mm\\ 0, & x<0.09mm\end{cases} \quad (13)$$

When the pintle moves back to the zero position (i.e. closed position), another barrier is enforced to simulate the supporting force from the bottom wall,

$$F_{bottom\ wall}(x)=\begin{cases}-K*x-c*\dot{x}, & x<0\\ 0, & x>0\end{cases} \quad (14)$$

Where K is the wall stiffness and K = 1e7 [N/m] for the current case; c is the damping coefficient and c = 1000 [N s/m] in this study.

The pressure force $F_{pressure}$ (*x, t*) on the pintle in vertical direction (i.e. pintle moving direction) was calculated using a CFD program in its transient simulation. This pressure force was also calculated statically at x=0 (i.e. pintle at its closed position) using the relation $F_{pressure}$ (*x* = 0) = *P* · A_x, where P is the fuel supply pressure (assuming uniform pressure within the fluid region) and A_x is the area in contact with fluid projected in the pintle moving direction. The static pressure force at different inlet pressures is shown in Figure 15. The pressure force, together with the initial spring and contact friction force, becomes the initial opposing forces that the magnetic force needs to overcome during the pintle opening event.

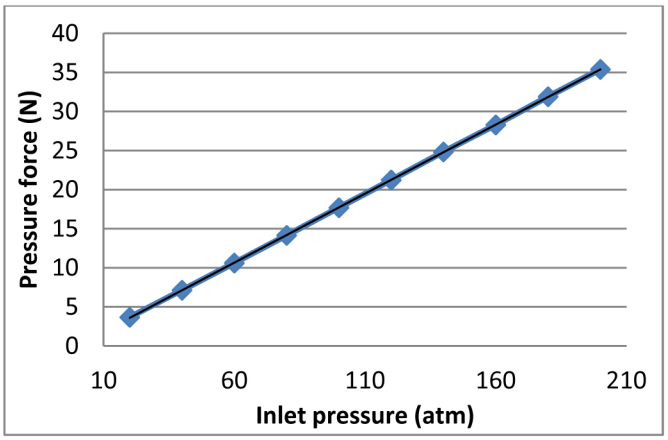

Figure 15. Calculated static pressure forces at pintle closed position at different inlet pressures

The pintle's equation of motion can be expressed as (ignoring damping of the fluid),

$$m\cdot\ddot{x}=F_{mag}(t)+F_{spring}(x)+F_{contact\ friction}(x)+F_{upper\ wall}(x)+F_{bottom\ wall}(x)+F_{pressure}(x,t) \quad (15)$$

All forces besides pressure force were incorporated into the rigid body dynamics as external forces in the CFD program. The pressure force was calculated at every time step in the transient simulation as the pintle position changed. In return, this pressure force was fed back to the rigid body motion as part of the external forces on the pintle. By doing so, the coupled electromagnetic-mechanical-fluid simulation was predicted.

Fluid System

Unlike other papers which included upstream pipe systems to consider pressure drops, mass transfer loss coefficients and pressure wave effects, this paper does not address the piping systems located away from the pintle. The effect of feeding pipe parameters on needle lift and flow rate can be found in [1], which investigated the impact of wave propagation on the injection event. Due to the scope of this paper, the rail dynamics' effect on pintle movement is not considered. But this can be an improvement of the fidelity of the fluid model in future study.

In this paper, the purpose of studying the fluid system was to investigate the pressure distribution around the nozzle and pintle valve during the pintle opening event. In order to ensure the accuracy of this fluid model, mass flow rates between calculated and measured data were compared at different inlet pressures. A sensitivity study of the nozzle diameter was performed to match the average mass flow rates. This multi-physics model was used to predict the injection spray event at different pressures and with different power strategies.

The CFD program used in this study was ANSYS CFX. The mesh preparation was done using the ICEM CFD mesh generation software. Only one sixth of the fluid region was modeled due to its periodicity. The pintle valve seat facets were simplified with smooth curvatures. A small inner radius was created instead of a singular point to make the mesh to be strictly hexahedral elements.

Mesh information is listed in Table 3. Typically, the quality of the mesh should be adequate for computation as long as the element angle is greater than 9~18 degrees and its determinant 2×2×2 is greater than 0.2. Different meshes were tested to study the mesh size effect on the mass flow rate at two different boundary conditions. Steady-state cavitation flow simulation at 200 atm supply pressure was carried out using different mesh sizes at pintle's fully open position. Figure 16 shows the mass flow rate tends to converge as the element number goes up. The mesh listed in Table 3 was found to be adequate to represent the geometry and generate convergent results.

The geometry of the modeled fluid region is shown in Figure 17.

Table 3. Mesh information for fluid model

Total elements	Total nodes	Lowest angle and the percentage	Lowest determinant 2x2x2 and the percentage
16097	12948	9~13.5 (0.703%)	0.25~0.3 (0.009%)

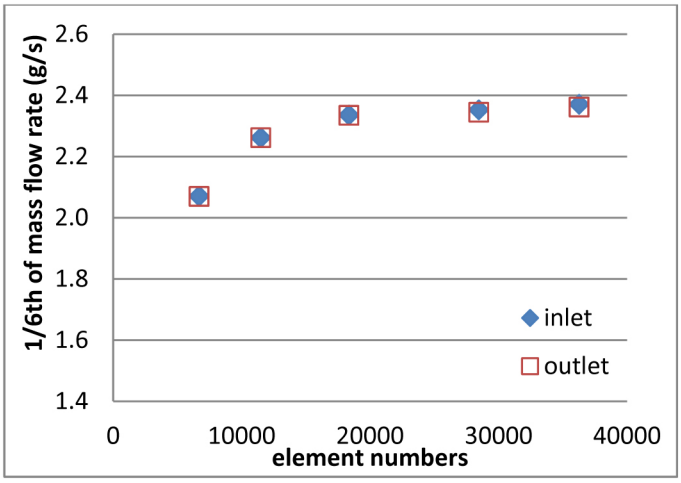

Figure 16. Grid independence study

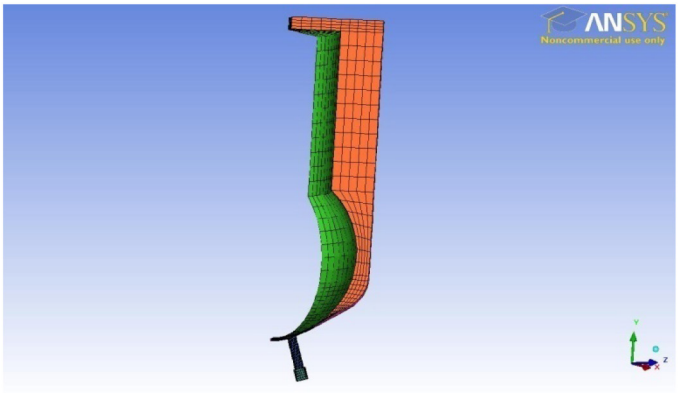

Figure 17. Meshed fluid region from ICEMCFD

Notice that this geometry only represents the initial fluid region. During the transient simulation in ANSYS CFX, the mesh will be deformed and the gap between the ball and valve seat will change. Since the software does not allow a zero or negative element, the complete separation of fluid region is not possible during the transient simulation. Therefore, a small gap (2.54e-3mm) was used to create the valve “closed” condition. The detail of this initial geometry at the ball valve location is shown in Figure 18.

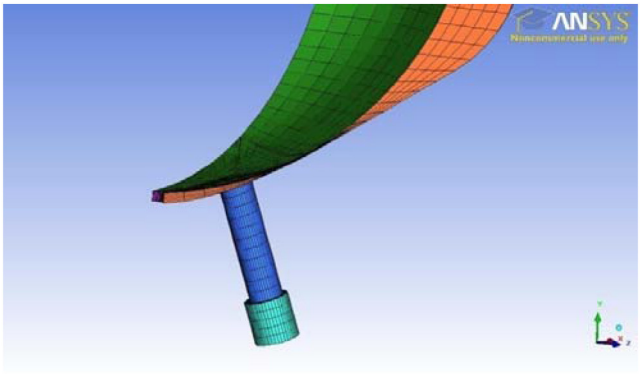

Figure 18. Small gap between ball and valve seat at the "closed" position

Transient cavitation flow simulation was performed in ANSYS CFX where a multiphase homogeneous model was used. In order to correlate with the experiments, Jet A fuel and air at 25°C were used as fluid and vapor phases, respectively. Jet A fuel was selected in the simulation because the injector power drive system optimization was performed for direct fuel injectors for military applications. Note that the saturation pressure of the Jet A fuel is 240 Pa. The fluid temperature was set at 25°C and the entire fluid region was assumed to be isothermal. The turbulence model was K-epsilon.

Mesh deformation strategy was used to incorporate rigid body motion in the transient simulation. The rigid body motion was applied to the pintle ball. The external forces on the ball were: spring force, electromagnetic force, initial contact friction force, and upper and bottom wall contact forces. The details of the force expressions were discussed in the previous section. Only a vertical (in the pintle moving direction) degree of freedom was allowed. Some key physical parameters are listed in Table 4.

Table 4. Key physical parameters for the fluid model

$1/6^{th}$ of the pintle mass	Pintle ball radius	Nozzle diameter	Initial pintle displacement
0.507 g	1.524mm	0.1524mm	2.54e-3mm

Boundary conditions, listed in Table 5, were specified as inlet, outlet and wall. Total and static pressures were used as inlet and outlet boundary conditions, respectively. The rest which includes the ball, valve seat, two periodic sides, and nozzle wall, were specified as no-slip wall boundary. The transient simulation's total run time was 2 ms and the time step was 0.25 μs.

Table 5. Boundary conditions

Inlet	Total pressure: 20 ~ 200 atm
Outlet	Avg. static pressure: 0 atm (reference pressure is 1 atm)
Others	No-slip wall

RESULTS AND DISCUSSIONS

Three different current shapes (power strategies) were used as the source of the pintle dynamics. The corresponding magnetic force profiles obtained using Maxwell was coupled with fluid model in ANSYS CFX transient. Pintle displacement, pressure force on the pintle and mass flow rate profiles during one injection event were obtained. The simulation revealed the details of the pressure forces' change with the pintle movement which led to the discovery of the magnetic force requirement for injection repeatability. This force requirement was further traced back in the Maxwell electromagnetic model to reveal the current shape requirement.

Two-stage current shapes were found to be the optimal power strategy for driving the fuel injector under different supply pressures. Key parameters, such as the 1^{st} stage current, the 1^{st} stage on-time, and the 2^{nd} stage current were obtained according to the magnetic force requirement. The optimization goal was to use the minimal current to drive the fuel injector and achieve repeatability under different supply pressures.

Finally, simulation results that showed successful operation under the optimal power strategy and simulation results that failed to operate the injector consistently were validated experimentally using a photo detector measurement system.

Power Strategy (a)

The current profile in Figure 7 was named as the power strategy (a) which was used in the simulation to understand the dynamics of the pintle and the pressure force during the pintle opening event. The results gave insights into the optimal power strategy to drive the fuel injector under different operating pressures.

The resultant magnetic force from Maxwell was expressed in Equation (10) which used the power strategy (a) current profile.

After running cases for different inlet pressures, three major results were obtained from ANSYS CFX transient simulation: pintle displacement, pressure force, and mass flow rate.

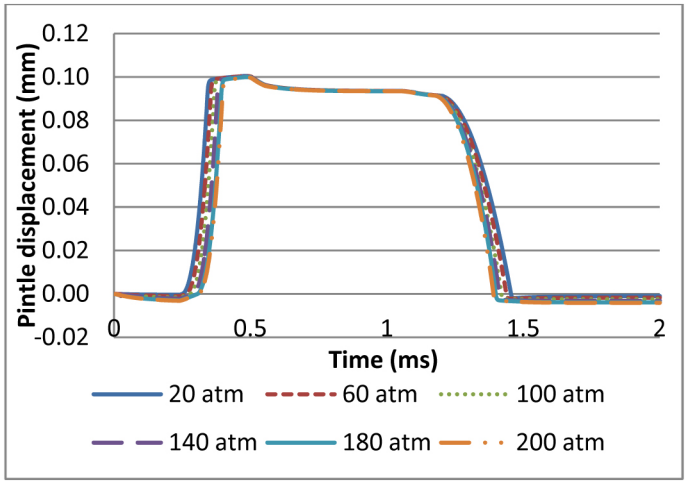

Figure 19. Pintle displacement profiles at different inlet pressures with power strategy (a)

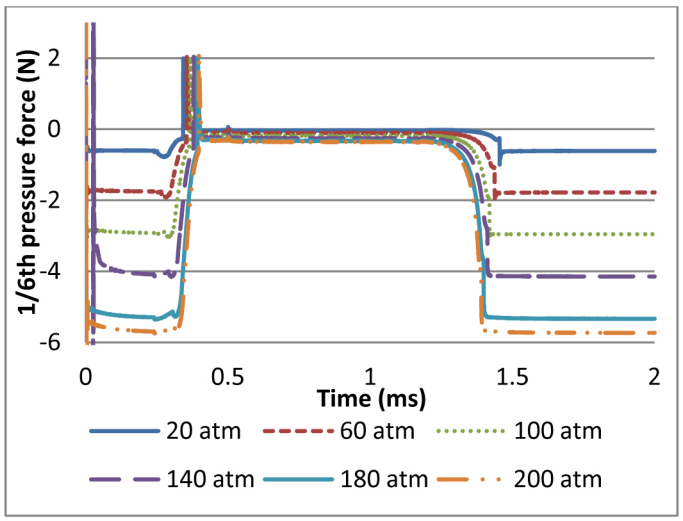

Figure 20. 1/6th of pressure forces on the pintle at different inlet pressures with power strategy (a)

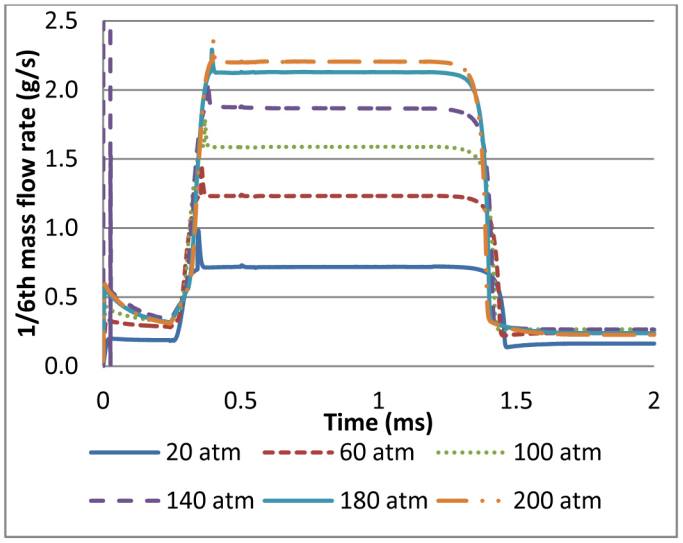

Figure 21. 1/6th of mass flow rates at different inlet pressures with power strategy (a)

As the inlet pressure was increased in Figure 19, the opening delay time became longer due to the increased initial pressure force on the pintle, as shown in Figure 20. This initial pressure force increased proportionally with the inlet pressure. As the current in the coil was built up (after the opening command signal), the magnetic force overcame the pressure force plus other resistant forces (i.e. spring force, contact friction force) and the pintle valve was opened. As the pintle moved, the pressure underneath the pintle ball increased, which caused the drop of net pressure force on the pintle ball. After the pintle reached its maximum position (upper wall of the stator), it hit the wall and was pushed back a little due to the stiffness of the wall. (Depending on the stiffness and damping coefficients, this could cause residual motion. For simplicity, this paper used a large damping coefficient to damp out this residual motion. The details of this phenomenon can be found in [2]. This push-back motion compressed the fluid region underneath the pintle ball, leading to a positive force spike as seen in Figure 20. After the pintle completely opened, it stuck to the upper wall of the stator and the pressure force on the pintle dropped to nearly zero. This was the time when steady flow formed, as can be seen from the “plateau” in Figure 21. In this figure, the mass flow rate was not strictly zero when the pintle was at its “closed” position due to the small gap used for the initial mesh. Regardless of this “leakage” flow at the “closed” position, the mass flow rate profile corresponded well with the pintle displacement profile.

In Figure 19, the pintle opening delay time started from 0.25 ms at 20 atm and increased to 0.31 ms at 200 atm. This increasing opening delay time was caused by the increasing initial pressure forces on the pintle ball as shown in Figure 20, from 3.6 N (total pressure force) at 20 atm to 35.4 N at 200 atm. Since the power strategy was the same, it took more time for the magnetic force to reach higher levels to overcome this increased initial pressure force. Therefore, in order to have minimum opening delay time, the 1st stage current increasing rate needed to be high so that it could reach the same current level with less time. Due to the limitation of the power supply's maximum voltage rating and the relation between the time to reach certain current level and supply voltage: $t \propto \frac{1}{V}$, the current increasing rate remained the same for all power strategies given the same voltage supply. Therefore, higher voltage rating power supplies are recommended for fast pintle opening.

After the current increasing rate was determined, the next question was how much current was required for the 1st stage to initiate the pintle opening. As discussed earlier in section 3, the magnetic force is needed to overcome the initial pressure, spring and contact friction forces. Table 6 listed the required magnetic forces at different inlet pressures. The relationship between the magnetic force and current was given in Figure 11. Using 0.1mm as the initial air gap and 160 as the number of coil turns in Maxwell, the corresponding threshold current levels were calculated using the force and current relationship

in Figure 11. The resultant threshold current values were listed on the far right column of Table 6. For example, it required 8.4 A to open the pintle valve in the case of 200 atm inlet pressure.

Table 6. Initial opposing forces, required magnetic forces and threshold current levels under different pressures

Inlet pressure (atm)	Initial pressure force (N)	Initial spring force (N)	Initial contact friction force (N)	Combined forces (required magnetic forces) (N)	Threshold current (A)
0	0	6.5	13.8	20.3	4.9
20	3.7	6.5	13.8	24	5.4
40	7.1	6.5	13.8	27.4	5.8
60	10.6	6.5	13.8	30.9	6.2
80	14.2	6.5	13.8	34.5	6.5
100	17.7	6.5	13.8	38	6.8
120	21.2	6.5	13.8	41.5	7.2
140	24.8	6.5	13.8	45.1	7.5
160	28.3	6.5	13.8	48.6	7.7
180	31.8	6.5	13.8	52.1	8.0
200	35.4	6.5	13.8	55.7	8.4

After this threshold current was determined for different inlet pressures, the next question was about the on-time of the 1st stage current. Although the threshold current was straight forward, the on-time of the 1st stage required careful observation from the pressure force profile shown in Figure 20.

As shown in Figure 20, the pressure force was the maximum when the pintle was at its “closed” position. As soon as the magnetic force overcame the initial opposing forces, this pressure force dropped dramatically to nearly zero. Depending on the supply fuel pressure, the pintle opening time varied a small amount. The time also varied only a small amount between when the pintle opened and when it reached the fully open position. This time duration between when pintle opened and when it reached the fully open position was important because only when the pintle reached the fully open position, did the steady flow form and the pressure force drop to nearly zero. And only when the pressure force dropped to nearly zero could we possibly drop the current to the 2nd stage holding current, which was only required to overcome the spring force.

If the 1st stage current dropped sooner than it required to keep the pintle motion going until it reached the fully open position, the pintle might experience early fall back due to the inadequate magnetic force compared to the combined pressure and spring force during this opening process. This created inconsistent injection. This situation was modeled using 0.25 ms on-time of the 1st stage current. We called this power strategy (b), with a current profile shown in Figure 22. The pintle displacement, pressure force and mass flow rate plots under power strategy (b) are shown in Figure 23, 24, 25.

Power Strategy (b)

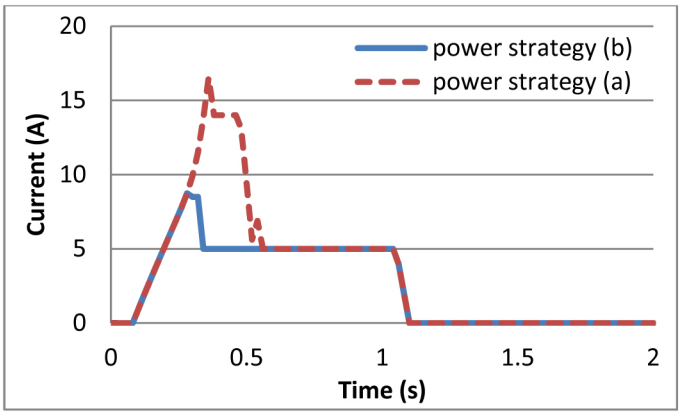

Figure 22. Current profile comparison between power strategy(a) and (b)

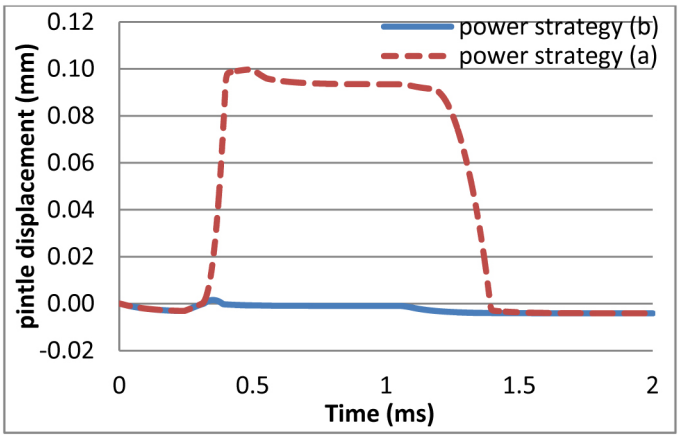

Figure 23. Pinlte displacement profiles with power strategy (b) and (a) at 200 atm supply pressure

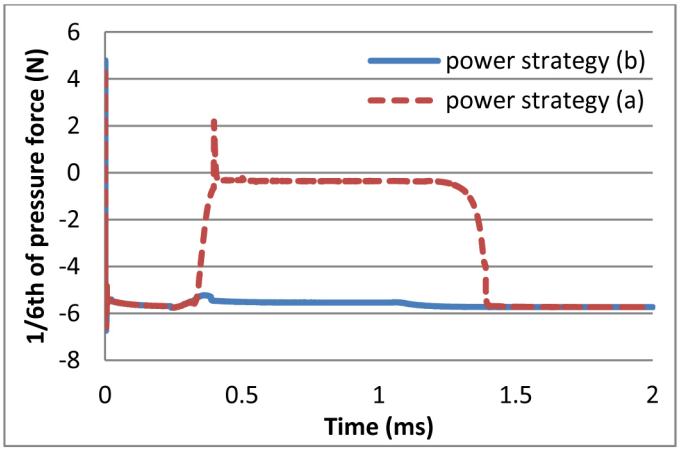

Figure 24. 1/6th of pressure forces on the pintle with power strategy (b) and (a) at 200 atm supply pressure

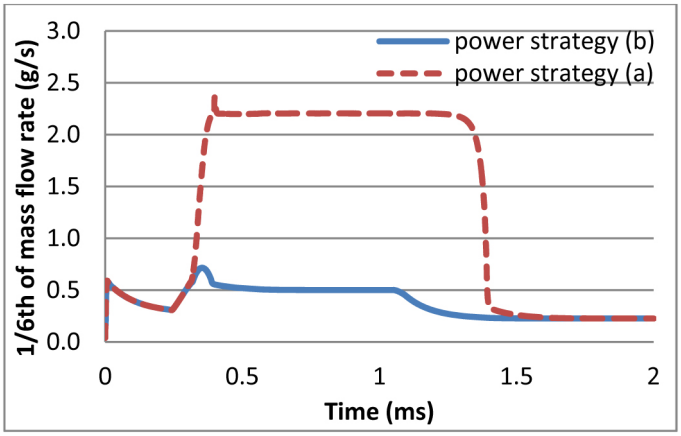

Figure 25. 1/6th of mass flow rates with power strategy (b) and (a) at 200 atm supply pressure

Power strategy (b) failed to completely open the pintle at 200 atm inlet pressure. The pintle was first initiated but it fell back before it reached the upper wall of the stator. Therefore, even though the 1st stage current level might be enough to overcome the threshold opposing forces (i.e. pressure force, spring force and initial contact friction force), it might create early fall (or random position) of the pintle as shown in the 200 atm inlet pressure, if the current dropped too soon (i.e. before the pintle reached the upper wall of the stator). This caused injection inconsistency. The ideal current of the 1st stage should remain at a certain level until the pintle reaches its maximum position to ensure consistency of fuel injection. The time that it took to fully open the pintle was estimated to be at most 0.4 ms based on the case with 200 atm supply pressure in Figure 20.

After the pintle was fully opened (i.e. the 1st stage), the magnetic force at the 2nd stage could be reduced significantly due to the drop of the pressure force at the pintle fully open position. Still, the magnetic force should be large enough to overcome the spring force at the pintle fully open position to hold the valve open. If the 2nd stage current level creates less magnetic force than the compressed spring force, the pintle might experience early fall as well. This is illustrated using current profile shown in Figure 26 which is named as power strategy (c). The pintle displacement, pressure force and mass flow rate plots with power strategy (c) under 200 atm supply pressure are shown in Figure 27, 28, 29.

With power strategy (c), pintle fell back earlier due to the inadequate 2nd stage magnetic force (at 3 A) to hold the pintle at its fully open position. Therefore, even though the 2nd stage current could be dropped, it required a minimum value (>3A, which created >7.5 N magnetic force at the fully open position. The spring force at the fully open position was 7.7 N) so that the magnetic force could still overcome the spring and pressure forces at the pintle fully open position. As discussed earlier, steady flow was formed and the pressure force dropped to nearly zero when the pintle was at its fully open position.

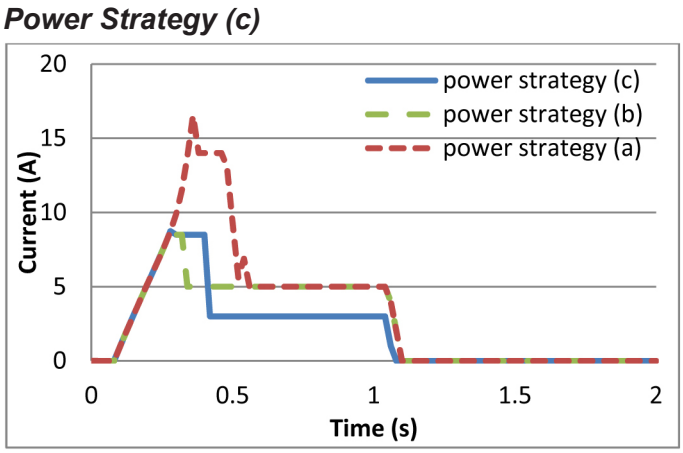

Figure 26. Current profile comparison among power strategy (a), (b) and (c)

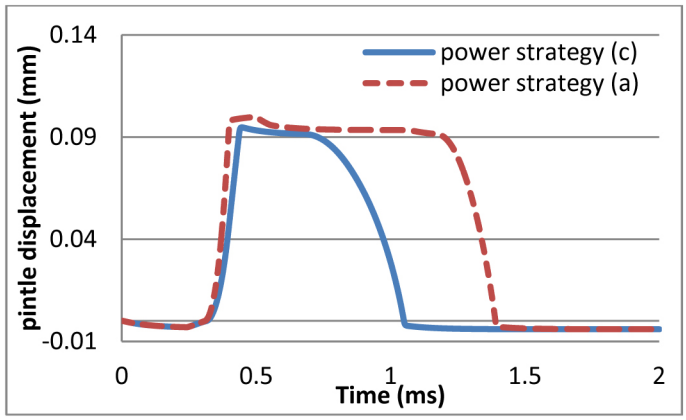

Figure 27. Pintle displacement profiles with power strategy (c) and (a) at 200 atm supply pressure

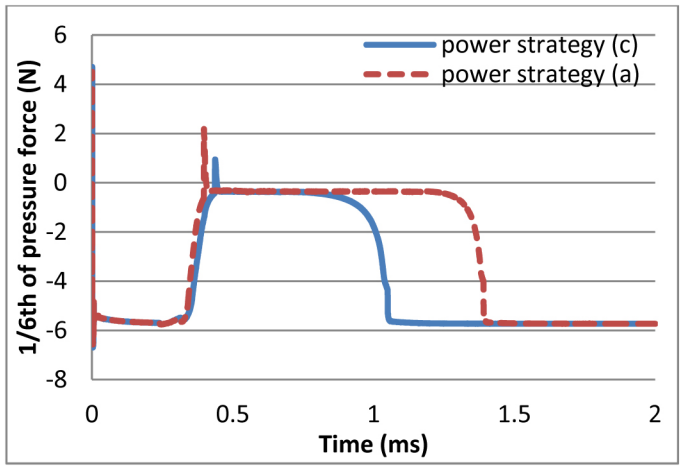

Figure 28. 1/6th of pressure forces on the pintle with power strategy (c) and (a) at 200 atm supply pressure

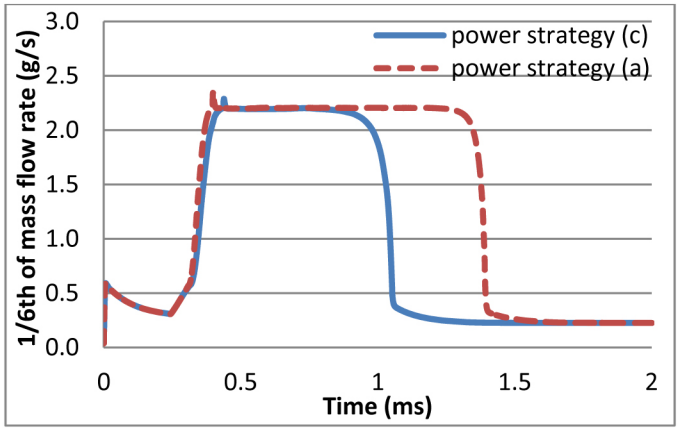

Figure 29. 1/6th of mass flow rates with power strategy (c) and (a) at 200 atm supply pressure

Optimal Power Strategy

After the trials of different power strategies, the magnetic force requirement that led to the current requirement gradually formed. From the previous discussion, there are three key parameters that determine whether or not the pintle could be successfully opened and held open: threshold current, the 1st stage on-time and the 2nd stage current.

These key parameters are illustrated in Figure 30. $I_{threshold}$ at different inlet pressures can be referred to Table 6. For example, $I_{threshold}$ = 8.4 A at 200 atm supply pressure.

$I_{pick-up}$ can be lowered based on the fact that once the pintle motion is initiated, the initial contact friction force drops to zero. $I_{pick-up}$ can be determined using the corresponding current value of the combined force minus the initial contact friction force at different inlet pressures in Table 6. For example, $I_{pick-up} \approx 7.5$ A at 200 atm supply pressure.

Ihold is the holding current for almost all pressure cases after pintle reaches the fully open position. Based on the spring force calculation (i.e. F_{spring} =7.7 *N* at pintle fully open position), the magnetic force at the pintle fully open position requires I_{hold} > 3 A. Refer to Figure 10 for ~0 mm air gap and steel 1008 case.

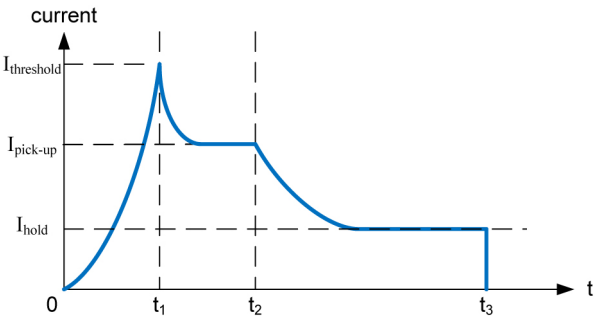

Figure 30. Current requirement illustration during one injection event

The three key current levels shown in Figure 30 are often mentioned as peak, pick-up and holding currents in the user's manual of fuel injectors. The previous discussion explained the reason for having these three key parameters. Threshold current is the current to overcome the initial contact friction, pressure force and spring force. Pick-up current is the current to keep the pintle opening motion going until it reaches fully open position. Holding current is the current to keep the pintle at its fully open position.

In a real application, the pick-up stage lasts a very short amount of time, the threshold and pick-up stages are often combined to form the 1st stage. Holding stage is to be called as the 2nd stage. Figure 31 illustrates how the current shape looks like for implementation.

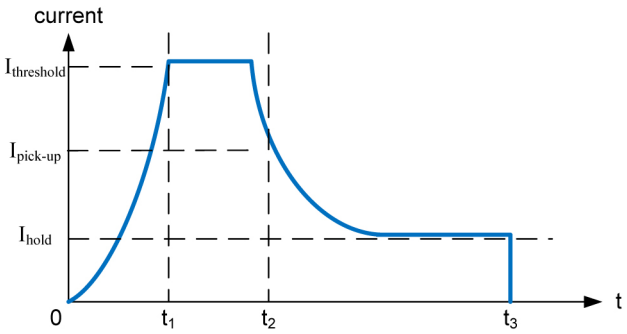

Figure 31. Current profile illustration for implementation

On the time axis, t_1 is the time when the pintle motion is initiated; t_2 is the time when the pintle reaches its fully open position; t_3 is the time when the injection is to be stopped. Among these times, t_2 is the time that ensures the pintle motion continues from when the motion gets initiated to the time when the pintle reaches its fully open position. This time is called the 1st stage on-time. It is around 0.4 ms based on the results from test and simulation. t_3 simply defines the total spray duration time. Despite the fact that the closing delay time is also closely related to pressure and magnetic forces (i.e. higher inlet pressure has the tendency to push the pintle back quicker, thus creating less closing delay time), it was found in the accompanying paper [9] that, the closing delay time is almost constant regardless of t_3, given adequate t_2 value and the spray duration time is proportional to total command signal on-time.

Validation

Validation Under Power Strategy (a)

JP-8 fuel was used in the validation experiment. JP-8 fuel was selected because the injector power drive system was designed to control a heavy fuel direct fuel injector for military applications. However, any other liquid fuel should be a sound substitute in the study. The test and simulation results on average mass flow rate during an opening event (total injection

quantity divided by injection duration time) were compared at different supply pressures in Figure 32. Power strategy (a) was used for all cases. The total injection quantity was measured by a scale after a specified number of injections.

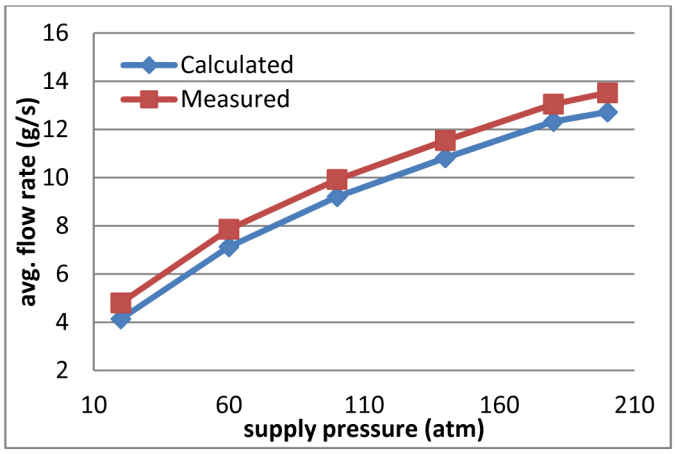

Figure 32. Average mass flow rate comparison during one injection event with power strategy (a) at different supply pressures

Accuracy of pintle displacement profiles was validated with the experimental data taken using a photo detector, which is an indicator of pintle motion. This approach assumes little time delay between the pintle motion and the detected spray. The discrepancy between the photo detector measured data and computer simulated pintle movement data are mainly due to this assumption. Overall, because of the high velocity spray under high supply pressure, the results from measuring the spray should give insights to the pintle behavior, which is the main purpose of this validation work.

The photo detector is an electronic device which emits an infrared beam to the receiver end. The change of the output of the receiver circuitry indicates whether or not there is an obstacle blocking the path. In our case, the fuel spray is the obstacle that causes the change of the photo detector output signal. The details of using the photo detector to measure the injection event can be found in the accompanying paper [9]. Figure 33 shows the control voltage, current and photo detector signal during an injection event with injection rate at 100 Hz. Four (4) volts of the photo detector output indicates no obstacles in the path, while nine (9) volts indicates obstacles are detected. Therefore, the “plateau” duration indicates the total spray duration time.

The spray temporal characteristics (i.e. opening delay and spray duration times) between calculated and measured data are compared in Table 7.

As shown in Table 7, the measured delay times did not follow the monotonous increasing trend of the calculated values as the supply pressure was increased. The discrepancy between the calculated and measured delay times was mainly due to the delay time between the first drop of spray coming out from the nozzle and the time when the photo detector sensed it. As the supply pressure was increased, the velocity of the first drop of spray increased as well. This shortened the delay time at higher pressures. Therefore, even though the pintle was opened quicker at lower pressures, it took longer time for the photo detector to detect the spray. The end result was about the same delay time (~0.4 ms) from photo detector measurement for all pressures.

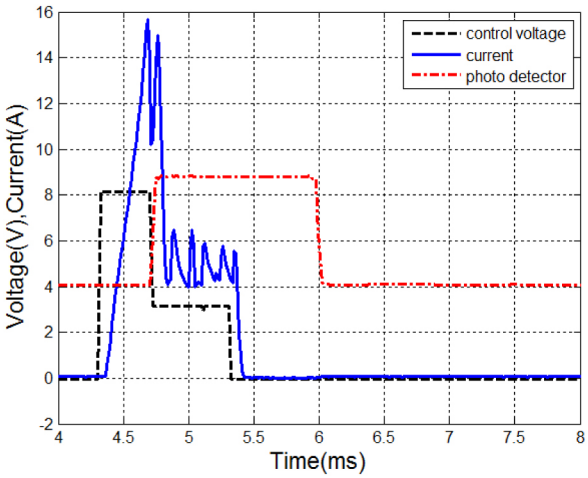

Figure 33. Test with photo detector during one spray event with power strategy (a) at 200 atm

Table 7. Spray temporal characteristics comparison between calculated and measured data

supply pressure (atm)	opening delay time (ms)		spray duration (ms)	
	calculated	measured	calculated	measured
20	0.25	0.43	1.21	1.25
60	0.27	0.41	1.17	1.31
100	0.28	0.39	1.14	1.31
140	0.29	0.39	1.12	1.30
180	0.31	0.39	1.09	1.28
200	0.31	0.40	1.08	1.28

The spray duration time followed the trend of calculated values at pressures higher than 20 atm. The discrepancy between the absolute values of the calculated and measured data was mainly due to the delay time when the pintle was closed and when the last drop of spray passed the photo detector. For the case at 20 atm supply pressure, the spray intensity was lower than its high pressure counterpart, this lowered intensity of the spray might render less stagnation time of the photo detector output.

Overall, there were small errors between the calculated and measured spray temporal characteristics (opening delay and spray duration times) due to the differences of pintle motion and spray detected at the photo detector. However, the close match of average mass flow rates and spray temporal characteristics at different supply pressures validates the multi-physics model during injector opening event.

Validation of Predicted Phenomena Under Power Strategy (b) and (c)

The purpose of the multi-physics model developed in this study was to optimize the power strategy to drive fuel injectors. This gave insights into the requirement of threshold current, the 1st stage on-time and the 2nd stage current. The multi-physics model predicted the failure of the power strategy (b) and (c). We then tested the injector using the similar power strategies and confirmed the inconsistency of the photo detector output, which was the indication of the early fall of pintle as we predicted in the simulation.

Figures 34 and 35 compare two power strategies with the same 1st stage current, 2nd stage current, total control signal on-time, but different 1st stage on-times. Figure 34 shows the consistency (same spray duration time between pulses) of the case with 0.3 ms 1st stage on-time, while Figure 35 shows the inconsistency (different spray duration times between pulses) of the case with 0.16 ms 1st stage on-time. The latter case is the demonstration of power strategy (b) in the simulation, which failed to open the pintle to its fully open position. The early fall back of the pintle was the cause of inconsistent spray duration times.

Figures 34 and 36 compare two power strategies with the same 1st stage current, 1st stage on-time, 2nd stage on-time, but different 2nd stage current levels. Figure 34 shows the consistency (same spray duration time between pulses) of the case with 3.5 A 2nd stage current, while Figure 36 shows the inconsistency (different spray duration times between pulses) of the case with 2.5A 2nd stage current. The latter case is the demonstration of power strategy (c) in the simulation, which failed to hold the pintle at its fully open position. The early fall back of the pintle was the cause of inconsistent spray duration times.

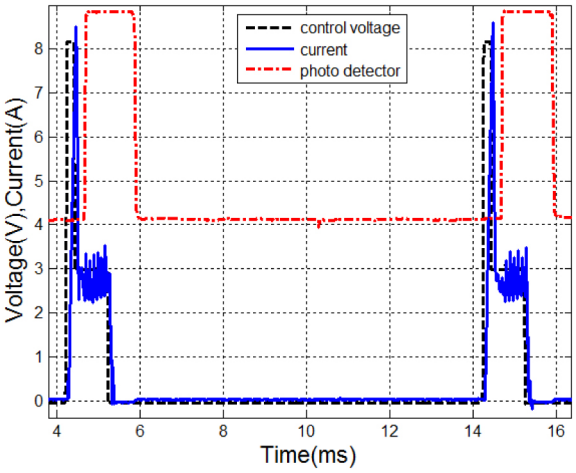

Figure 34. Photo detector output with 1st stage current of 8 A, 1st stage on-time 0.2 ms, 2nd stage current of 3.5 A, 2nd stage on-time 0.8 ms; at 200 atm supply pressure

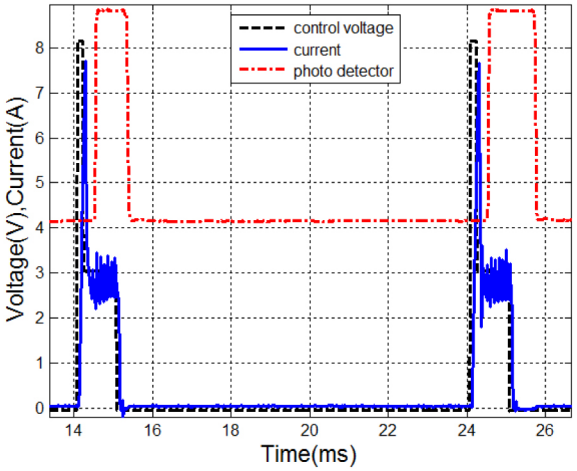

Figure 35. Photo detector output with 1st stage current of 8 A, 1st stage on-time 0.16 ms, 2nd stage current of 3.5 A, 2nd stage on-time 0.84 ms; at 200 atm supply pressure

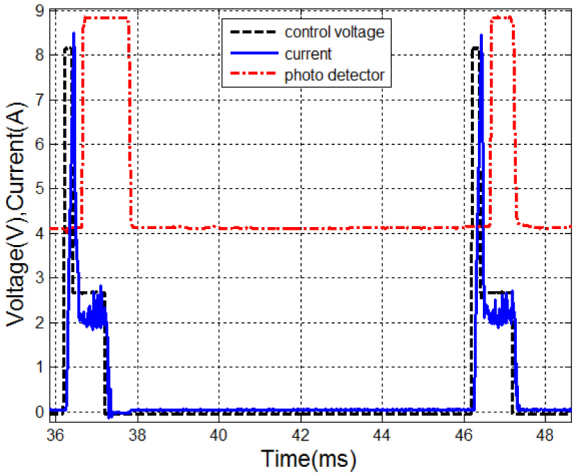

Figure 36. Photo detector output with 1st stage current of 8 A, 1st stage on-time 0.2 ms, 2nd stage current of 2.5 A, 2nd stage on-time 0.8 ms; at 200 atm supply pressure

CONCLUSION

This paper presents a coupled electrical-electromagnetic-mechanical-fluid model of a direct fuel injector and its power drive system. A simplified electrical circuit model was built to create the current profile to the injector coil from a two-stage PWM current controlled approach. The circuit model was then imported into the finite element code Maxwell for an electromagnetic force calculation. Pintle transient movement and the non-linearity of B-H curve were considered in the model. The force calculated using Maxwell was compared with the 1D electromagnetic analysis. Then, the magnetic force profile was obtained with power strategy (a). A detailed mechanical model, which included rigid body motion of pintle, spring force, initial contact force, pressure force and spring-damper system as wall barrier, was formed. One-sixth of the coupled electromagnetic-mechanical-fluid model using the

CFD code ANSYS CFX was built and analyzed. Pintle displacement, pressure force and mass flow rate transient responses were obtained. The pressure force gave insights into the power requirement during the pintle opening event. Different power strategies were used in the computer model to illustrate the cause of injection inconsistency. Finally, a photo detector based spray temporal measurement system was used to validate the results from computer simulation.

The optimal power requirement for a two-stage PWM current controlled approach was obtained to improve the injection repeatability at minimum power consumption:

1. The 1st stage current needs to be able to overcome initial opposing forces such as spring, pressure and contact friction force ($I_{threshold}$ > 8 A at 200 atm supply pressure). The threshold current can be lowered at lower operating pressures. It is always recommended to use higher voltage rating power supplies for fast pintle opening.
2. The 1st stage on-time needs to be long enough to keep the pintle movement going until it reaches its fully open position ($t_2 \approx 0.4$ ms). Otherwise the pressure force will push the pintle back to create early fall back, which is one cause of injection inconsistency;
3. The 2nd stage current can be lowered significantly due to the drop of pressure force at pintle fully open position, yet it needs to maintain at certain level to be able to overcome the spring force and hold the pintle at its fully open position (I_{hold} > 3 A). Otherwise the pintle will experience an early fall as well due to the spring force, which is another cause of injection inconsistency. The 2nd stage current requirement does not increase as the supply pressure increases due to the fact that once the pintle is at its fully open position, the steady flow forms and the pressure force on the pintle drops to nearly zero.
4. The 2nd stage on-time has not been discussed due to the fact that the closing delay time does not vary with on-times and the total injection time is proportional to control signal's total on-time. The injection time can be easily adjusted by changing the 2nd stage on-time.

The fluid model used in this paper only included geometries at the near-nozzle region. The upstream piping system was not considered in the model. Furthermore, due to the inaccessibility of the real-time pintle displacement, pressure force on the pintle and flow rate measurement, only average flow rate data and photo detector data (indicator of pintle displacement) were used to validate the results from computer simulation. More careful matching of these instantaneous profiles is needed for future investigation.

This paper also has given insights into how to design a high-performance fuel injector:

1. High magnetic saturation material is preferred to build fuel injectors to create larger magnetic force to initiate the pintle motion.
2. The return force (spring force in this study) determines the closing delay time. Thus, large return force would create less closing delay time.
3. The fluid model can be used to better understand the physics during the fuel injection. For example, the relationship between nozzle diameter and mass flow rate; the effect of geometry changes on the cavitation zone at various operating pressures. The cavitation can thus be reduced or eliminated by carefully choosing the right geometries and pintle motions.

ACKNOWLEDGEMENTS

The authors acknowledge the Texas A&M Supercomputing Facility (http://sc.tamu.edu/) for providing computing resources (ANSYS CFX and meshing tool ICEMCFD) in conducting the research reported in this paper. The authors would also like to thank Dr. James T. Edwards (Air Force Research Laboratory) for providing the JP-8 test fuel.

REFERENCES

1. Digesu, P. and Laforgia D., “Diesel electro-injector: A numerical simulation code”. Journal of Engineering for Gas Turbines and Power- Transactions of the Asme, 117(4): 792-798, 1995. Doi10.1115/1.2815466.
2. Ficarella, A. and Laforgia D., “Experimental and numerical investigation on cavitating flows in diesel injection systems”. Meccanica, 33(4): 407-425, 1998. Doi10.1023/A:1004329902598.
3. Coppo, M., Dongiovanni C., and Negri C., “Numerical analysis and experimental investigation of a common rail-type diesel injector”. Journal of Engineering for Gas Turbines and Power- Transactions of the Asme, 126(4): 874-885, 2004. Doi10.1115/1.1787502.
4. Coppo, M. and Dongiovanni C., “Experimental validation of a common-rail injector model in the whole operation field”. Journal of Engineering for Gas Turbines and Power-Transactions of the Asme, 129(2): 596-608, 2007. Doi10.1115/1.2432889.
5. Hu, Q., et al., “Modelling of dynamic responses of an automotive fuel rail system, part I: Injector”. Journal of Sound and Vibration, 245(5): 801-814, 2001. Doi10.1006/jsvi.2000.3605.
6. Ando, R., Koizumi M., and Ishikawa T., “Development of a simulation method for dynamic characteristics of fuel injector”. Ieee Transactions on Magnetics, 37(5): 3715-3718, 2001. Doi10.1109/20.952697.
7. Tsai, W.C. and Yu P.C., “Design of the Electrical Drive for the High-Pressure GDI Injector in a 500cc Motorbike Engine”. International Journal of Engineering and Industries, volume 2, Number 1, March, 2011. doi:10.4156/ijei.vol2.issue1.9.
8. Tsai, W.C. and Wu Z.H., “Use of Taguchi Method to Optimize the Operating Parameters of a High-Pressure Injector Driving Circuit”. Mechanical and Electronics Engineering Iii, Pts 1-5, 130-134: 2795-2799, 2012. Doi10.4028/www.scientific.net/AMM.130-134.2795.
9. Zhang, X., Palazzolo, A., Kweon, C., Thomas, E. et al., “Direct Fuel Injector Temporal Measurements,” SAE Technical Paper 2014-01-1444, 2014.

1 (PDF) DEFENSE TECHNICAL INFORMATION CTR DTIC OCA

2 (PDF) DIRECTOR US ARMY RESEARCH LAB RDRL CIO LL IMAL HRA MAIL & RECORDS MGMT

1 (PDF) GOVT PRINTG OFC A MALHOTRA

1 (PDF) DIR USARL RDRL VTP C KWEON

INTENTIONALLY LEFT BLANK.